Towards the Development of Low Power Arcjet for Use with Green Propellant

Trevor M. Moeller[1]

University of Tennessee Space Institute, Tullahoma, TN, 37388, USA

Conventional arcjet propellants are hydrazine and ammonia. Both are toxic and environmentally unfriendly, requiring the use of complicated handling logistics and increased cost. If successfully demonstrated in arcjets, the use of green propellants would alleviate these issues. This paper details improvements made to the design of a low-power arcjet to be used in testing. Diagnostic tools to be used to assess thruster performance were also developed. These include emission spectroscopy for the detection of thruster insulator erotion and a two-cord heterodyne laser interferometer for measure electron number densities and estimate the exit velocity of the propellant.

Nomenclature

c	=	speed of light in vacuum
$D12$	=	distance between lens 1 and lens 2
$D23$	=	distance between lens 2 and lens 3
ϵ_o	=	permittivity of free space
$f1$	=	focal length of lens 1
$f2$	=	focal length of lens 2
$f3$	=	focal length of lens 3
$I1$	=	image of lens 1
$I2$	=	image of lens 2
$I3$	=	image of lens 3
λ	=	wavelength
l	=	length along laser beam
$L1$	=	lens 1
$L2$	=	lens 2
$L3$	=	lens 3
$M1$	=	magnification of lens 1
$M2$	=	magnification of lens 2
$M3$	=	magnification of lens 3
M_e	=	electron mass
M_{total}	=	magnification of lens system
n'	=	index of refraction
$O1$	=	object of lens 1
$O2$	=	object of lens 2
$O3$	=	object of lens 3
φ	=	phase shift
q	=	charge on electron
$S1$	=	distance between lens 1 and its object
$S2$	=	distance between lens 2 and its object
$S3$	=	distance between lens 3 and its object
$S1'$	=	distance between lens 1 and its image
$S2'$	=	distance between lens 2 and its image
$S3'$	=	distance between lens 3 and its image

---

[1] Associate Professor, Department of Mechanical, Aerospace and Biomedical Engineering, MS 24, AIAA Associate Fellow.

American Institute of Aeronautics and Astronautics

I. Introduction

ARCJETS are electric propulsion devices that generate thrust through the thermal expansion of the propellant, just like a chemical rocket. However, the thermal energy in the propellant of the former is not limited by the combustion of an oxidizer and fuel; Ohmic heating provides much higher propellant temperatures, resulting in higher specific impulse leading to a reduced propellant requirement for the same mission. For this reason arcjets have found wide use for station keeping on satellites. Arcjets on satellites traditionally use hydrazine (N_2H_4) as a propellant, as it is a monopropellant that releases heat when decomposed with a catalyst, and it has a relatively low mixture molecular weight (5.333 g/mole). Unfortunately, hydrazine is hazardous to people and the environment. Green propellants have low toxicity and offer high-performance and high-efficiency compared to conventional chemical propellants[1]. Successful demonstration and adoption of a green alternative for arcjet propellant would greatly reduce propellant handling procedures and logistics[2].

II. Thruster Hardware

Arcjets are comprised of an anode and a cathode separated by an electrical insulator. The flowpath in the anode forms a Laval nozzle that produces supersonic flow in the diverging nozzle (Figure 1a). Propellant is introduced tangential to the anode wall, upstream of the constrictor (nozzle throat) to form a swirling flow. An arc extends from the tip of the cathode, through the constrictor, to the diverging portion of the anode. The swirling propellant flow stabilizes the arc by promoting a cool boundary layer with low electrical conductivity close the the constrictor wall (Figure 1b). In an ideal arcjet, the anode attachment is a diffuse arc that attaches symmetrically to the expanding nozzle. In reality the arc attaches in one location that rapidly moves circumferentially.
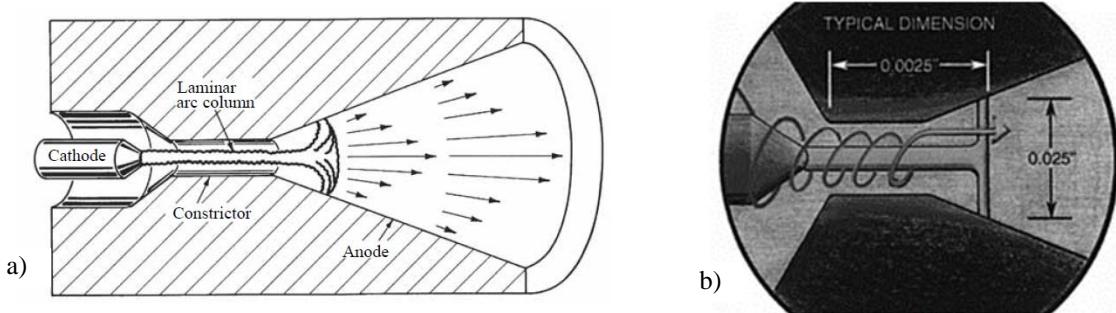

Figure 1. Arcjet schematic and propellant flow through arcjet[3,4]

The arcjet thruster on which the green propellant will be demonstrated is designed to operate at 1 kW. The constrictor is 0.040 inches in diameter and 0.040 inches long (Figure 2). The diverging nozzle is conical with a 22.5 degree half angle. The cathode tip is a 25 degree half-angle cone. Propellant enters the arcjet through a fitting near the breech of the insulator and flows into a manifold that feeds six channels to the nozzle (Figure 3). At the end of each channel, the flow enters a 1/32 inch hole that ends at the wall upstream of the constrictor (see inset in Figure 3). This creates a swirling flow. A photo of the assembled arcjet appears in Figure 4.

Past tests of this arcjet operating with argon propellant resulted in disappointing performance. The argon propellant is not a good propellant for electrothermal devices, and the cathode-anode spacing for the arcjet operating conditions resulted in the electrodes being welded together. It was decided to operate arcjet on hydrogen-nitrogen mixtures that represent dissociated ammonia (NH_3) and dissociated hydrazine (N_2H_4), conventional arcjet propellants, before moving to a green propellant. These tests would provide a baseline for the arcjet performance.

During the period of performance of the present effort, the insulator was redesigned to introduce the propellant tangentially along the anode wall to provide a swirling flow that will reduce arc instabilities in the constrictor (Figure 2. After fabrication the arcjet was assembled. While inserting the cathode into the assembly, it became bound and the insulator cracked. Schedules did not permit fabricating a replacement. Before fabricating a replacement in the future, it is recommended that the insulator design be updated for a loose fit hole for the cathode to allow for easier assembly and cathode thermal expansion during operation. It also is recommended to use a 0.063 inch radius ball end mill to fabricate the manifold that feeds the propellant channels in the insulator. This will reduce stress at the location where the insulator cracked on multiple occassions.

American Institute of Aeronautics and Astronautics
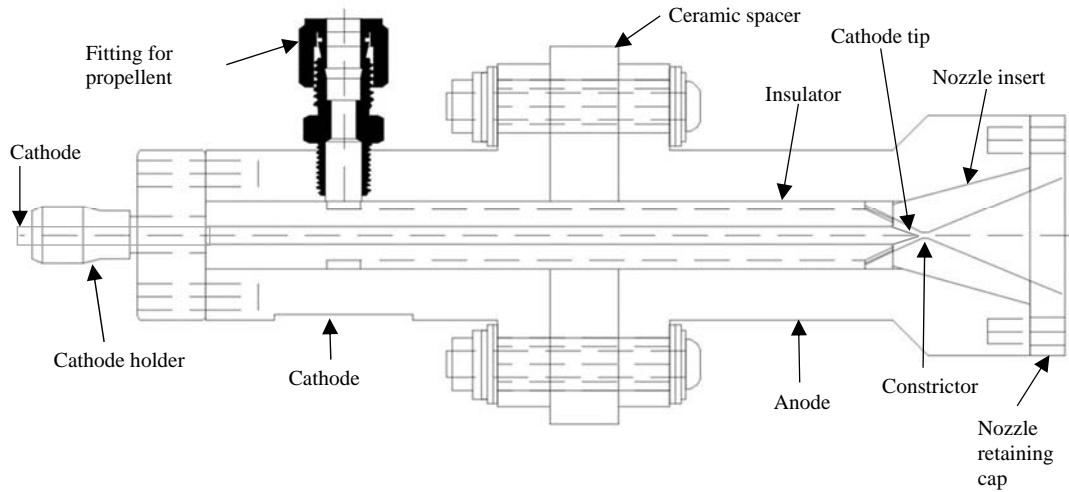
Figure 2. Arcjet assembly

Figure 3. Ceramic insulator with propellant feed channels.

a)   b)   c)
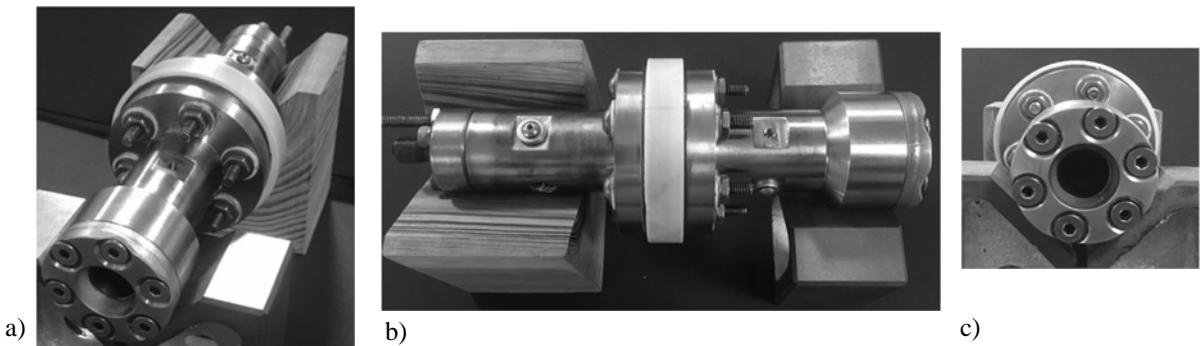
Figure 4. a) Oblique, b) Top, and c) Front view photos of the assembled arcjet.

3

American Institute of Aeronautics and Astronautics

III. Diagnostics

Emission spectroscopy and heterodyne laser interferometry diagnostic systems were developed. These diagnostics can be used to provide measurements of electron number densities, electron temperature, and species concentrations.

A. Emission Spectroscopy

Atoms and molecules have unique spectra lines associated with transitions between electronic states, and molecules have additional transition structures associated with vibrational and rotational states. When the energy level of the initial state is greater than that of the final state, a photon with energy $h\upsilon$ is released. Transitions between select states in the atom or molecule result in a spectrum of lines that are unique to that atom or molecule. Hence, the spectral emission of radiation can be used to determine the constituents of a plasma. Measurement of spectral line widths provide information on specie concentrations, and line intensities can be used to determine electron temperatures[5,6].

A schematic of the emission spectroscopy setup as a thruster diagnostic is shown in Figure 5. In the present application, an image of the desired thruster plume area is directed into the the entrance slit of an Acton SP-500i, 0.5 m Czerny-Turner spectrometer. The optics used to produce the image (described below) were selected to almost fill the entrance slit, allowing spatial resolution of spectral emission. The instrument used to collect the spectral image depends on the wavelength of interest. A Princeton Instruments PI-MAX Camera is available for data acquisition in the visible part of the spectrum. It has an intensified, square CCD detector that can provide spatially resolved spectra from the spectrometer. For spectra in the near UV the spectrometer is converted to a monochrometer by fitting it with an exit slit, and a photomultiplier tube sensitive in the UV is used to measure emission intensity as the spectrometer is scanned through the desired spectral range.
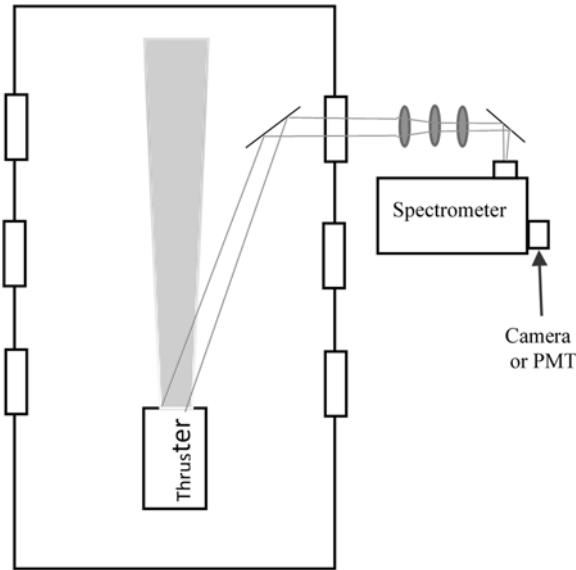

Figure 5. Schematic of setup for emission spectroscopy

A three-lens system, shown schematically in Figure 6, was developed to image the discharges from a pulsed inductive thruster (PIT) and asmall PIT. The small PIT configuration should be suitable for use with the arcjet. Because the object, *O1*, is much larger than the height of the spectrometer entrance slit, expanding (concave) lenses, *L1* and *L2*, are used to produce a virtual image, *I2*, that is focused onto the entrance slit by a converging (convex) lens. Thin lens theory[4] was used to aid the design process.

American Institute of Aeronautics and Astronautics
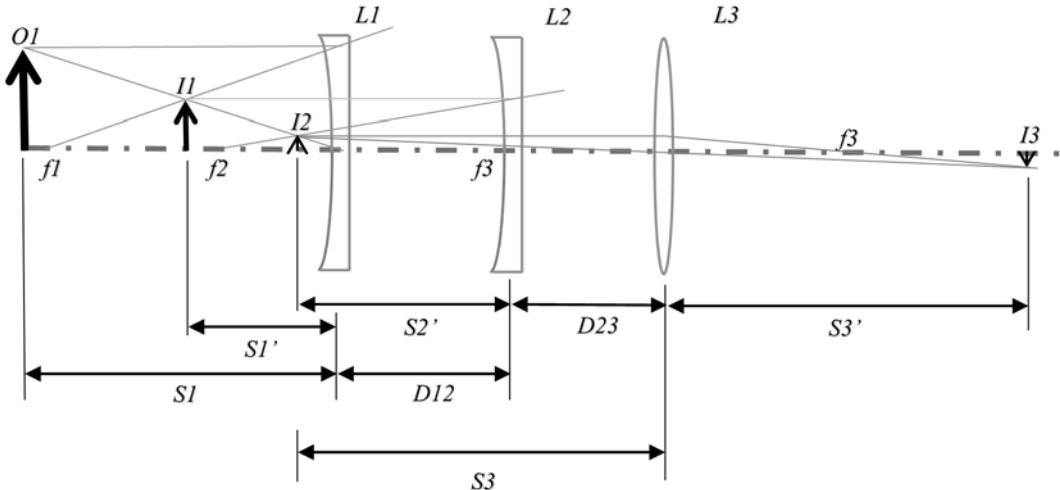
Figure 6. Three-lens imaging system

In a multiple lens arrangement the image of an object from the first lens becomes the object of the second lens, whose image becomes the object of the third lens, and so on. Thin lens equations[7] can be used to determine the image position, when the object postion relative to the lens and the focal length are known. The location of the first image, *S1'*, is given by:

$$S1' = \frac{S1 \cdot f1}{S1 - f1} \tag{1}$$

The location of the object for the second lens, *S2*, relative to *L2* is:

$$S2 = D12 - S1' \tag{2}$$

Note that the focal length for a concave lens is negative, and the distance to the image to a lens is negative with the image is on the left hand side of the lens. Hence the negative sign is used for our case. The image from the first lens, located at *S2*, is the object of the second lens. The location of the image that results from the second lens is given by:

$$S2' = \frac{S2 \cdot f2}{S2 - f2} \tag{3}$$

This image is the object for the third lens. The location of the object with respect to lens 3 is given by:

$$S3 = D23 - S2' \tag{4}$$

Note again that the the negative sign in the preceeding equation results accounts for the negative focal length of the second lens in our case. The final image will be located at *S3'* with respect to the third lens.

$$S3' = \frac{S3 \cdot f3}{S3 - f3} \tag{5}$$

The total distance from the object, *O1*, to the final image is given by

$$D_{total} = S1 + D12 + D23 + S3' \tag{6}$$

To ensure that the image of the object falls within the height of the spectrometer entrance slit, the magnification of the three-lens system must be determined. The total magnification, M_{Total}, of a series of lenses is simply the product of the magnification for the individual lenses. For our case,

$$M_{total} = M_1 \cdot M_2 \cdot M_3 \tag{7}$$

5

American Institute of Aeronautics and Astronautics

where

$$M_1 = -\frac{s_1'}{s_1}; \quad M_2 = -\frac{s_2'}{s_2}; \quad M_3 = -\frac{s_3'}{s_3} \qquad (8)$$

Equations (1) through (8) were entered into a spreadsheet to calculate the total magnification, image height, and position of the image of lens 3 given the object height, the distance between the object and lens 1, distances between the lenses, and the focal lengths of the lenses. Two scenarios are envisioned for imaging a thruster, one for larger thrusters and one for smaller thrusters. The PIT and small PIT are reasonable examples, respectively. For the PIT, the plasma region of interest is approximately 30 cm tall and would be positioned approximately 4 m from the spectrometer. For the small PIT, these values are 9 cm and 2 m. Parametric studies using lenses available from Newport were conducted in an attempt to optimize the optical configuration to achieve a final image height approaching 1.4 cm, the height of the spectrometer entrance slit, and a non-expanding image entering the spectrometer. The latter is accomplished by positioning the object of the convex lens, L3, two focal lengths from lens 3. Because of the spacing constraints and the limited availability of negative focal length (concave) lenses, a configuraton meeting both criteria could not be achieved. This was especially true for imaging the small PIT plume (see Table 1). Note that the negative sign in the image height indicates the image is inverted. Also note that the first two rows of data. Rows 3 and 4 are not ideal, but use lenses that are in-stock, allowing the optical setup concept to be tested earlier. The total distance from the object to the entrance slit is significant enough to require turning mirrors with antireflection coatings for the UV range, and the total distance can be altered significantly while maintaining a reasonable image height.

Table 1. Parameters of optical setup

Object Height (mm)	f1 (mm)	f2 (mm)	f3 (mm)	S1 (mm)	D12 (mm)	D23 (mm)	S3' (mm)	Dtotal (mm)	Image Height (mm)
300	-500	-500	150	4000	300	50	351	4700	-13.46
93.3	-500	-500	150	2000	30	70	299	2399	-9.95
300	-250	-250	100	4000	140	50	208.3	4398	-6.66
90	-200	-250	75	2000	30	25	162	2217	-5.33

Erosion of the boron nitride (BN) electrical insulators typically used in electric propulsion devices makes it is of interest to monitor boron emission lines in the thruster exhaust. Since the preliminary testing of the PIT is done in open air, nitrogen emission lines cannot be used. There are no strong atomic boron lines in the visible part of the spectrum. However, there are strong boron lines at 249.6769 nm and 249.7722 nm [8] in the ultraviolet, thus requiring optics with antireflective coatings for UV wavelengths. Either a UV-sensitive intensified camera or a UV-sensitive photomultiplier tube must be used to detect these lines. An alternate approach would be to use barium (Ba) as a dopant placed on the surface of the BN insulator, since it is an element not likely to be present in the local environment. Also, atomic barium has a strong emission line in the visible at 553.5481 nm [8]. There appear to be no nitrogen or oxygen lines near this wavelength, so the barium line should be discernable, if present. The spectrometer can be spectrally calibrated in this region of the spectrum using a neon/mercury calibration lamp, which has the following lines on either side of the line of interest: NeI 540.05618 nm, HgI 546.0735 nm, NeI 576.4418 nm, and NeI 585.24879 nm [8].

At the end of the period of performance the spectral emission diagnostic was near completion. The spectrometer was calibrated in the visible spectrum using a high-speed camera with intensified detector. Calibration in the UV, where atomic boron lines reside was near completion. For the UV, a high-speed camera with intensified detector was installed, but unfortunately it appeared to malfunction and could not detect lines in either the UV or visible. As an alternate to using the camera for detection, the spectrometer was transformed into a monochrometer through the installation of an exit slit to which a photomultiplier tube (PMT) was mounted. Only vintage PMT equipment was available, and missing components prevented the completion of this diagnostic tool before the end of the period of performance.

To provide the capability to collect spatially-resolved spectral emission across a region of a thruster plume, a three-lens imageing system was designed, as described above. Multiple lens configurations were recommended to allow imaging the desired areas of thruster of different sizes. Lenses were ordered, but many still were on backorder at the completion of the period of performance.

American Institute of Aeronautics and Astronautics

B. Heterodyne Laser Interferometry

Interferometry has long been used as a non-intrusive tool for plasma characterization[9], providing a means of determining line of site electron number density. The refractive index, n', due to electrons in a plasma is related to the electron number density, N_e, [10]

$$n' - 1 = -\frac{\lambda^2 N_e q^2}{8\pi^2 m_e \epsilon_o c^2} \tag{9}$$

The resulting phase shift is given by

$$\varphi = -\frac{2\pi}{\lambda} \int (n' - 1)\, dl \tag{10}$$

Substitution of equation (9) into equation (10) gives

$$\varphi = -\frac{\lambda q^2}{4\pi^2 m_e \epsilon_o c^2} \int N_e\, dl \tag{11}$$

Thus, one can determine the electron number density integrated over a line of site through a plasma by measuring the phase shift. This is accomplished by splitting a laser beam, passing the field beam through a plasma and recombining the beam with the reference beam to produce constructive and destructive interference that results in interference fringes. Laser interferometer techniques are all based on this principle but very in arrangement.

For the work described herein heterodyne laser interferometry with electronic quadrature phase detection was used. The heterodyne laser interferometer was introduced by Weber[11,12]. A schematic of a single cord, heterodyne laser interferometer in a Mach-Zehnder configuration is shown in Figure 5. A 17 mW helium-neon laser with a 632.8 nm beam is split into a reference beam and a field beam with a pellicle beam splitter (BS in Figure 7). The field beam is modulated by an acousto-optic modulator (AOM), which adds a sinuosoidal phase modulated intensity to beam modes greater than one. The first mode (dashed line in Figure 3) is isoloated and used for the field beam, which passes through the plasma and is recombined with the reference beam via a beam splitter before illuminating the detector (D). The reference beam (solid line in Figure 7) has an optical path length that can be varied using the translation stage (TS). Laser interferometers are commonly configured so that the reference and field beams have the same length, ensuring the coherence of the beams. However, in Ref. 13 it is shown that it is not necessary to have equal path lengths, but the path length difference must be an even multiple of the laser cavity length.

The single chord heterodyne laser interferometer shown in Figure 7 can be used to measure line of site electron number density using equation (11). The background phase shift, the phase shift of the setup without plasma present, provides the measurement uncertainty. The two chord heterodyne laser interferometer shown in Figure 8 has two field beams that can be used to determine the line of sight electron number density at two distinct locations. They also allow the determination of the directed velocity of the electrons from the known distance between the chords and the time it takes to traverse the distance. For large vacuum chambers, the setup shown in Figure 8 is not practical, as it becomes difficult to direct beam paths around the chamber without obstruction. An alternate setup for large chambers is shown in Figure 9. It provides a simpler optical setup by incorporating two-passes of the field beam through the chamber for each cord. The configuration shown in Figure 8 was set up and demonstrated, and photographs are provided in Figure 10.

American Institute of Aeronautics and Astronautics
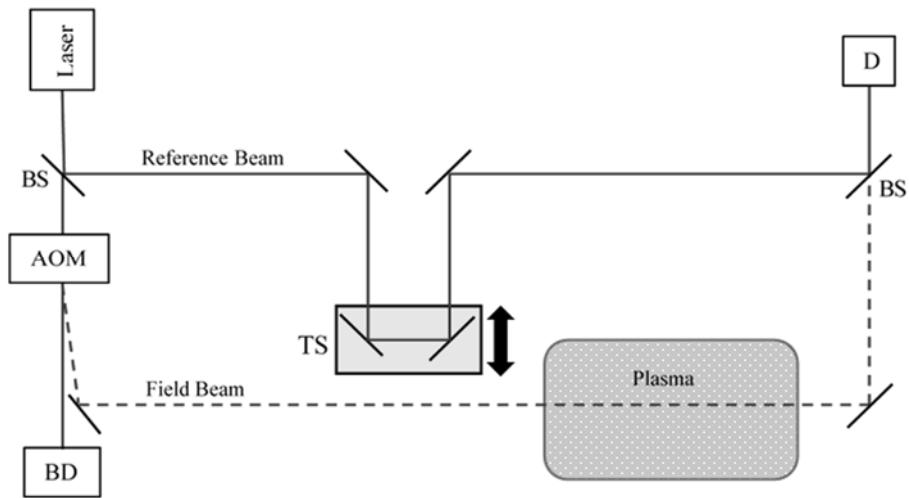
Figure 7. Schematic of heterodyne laser interferometer setup (single cord)
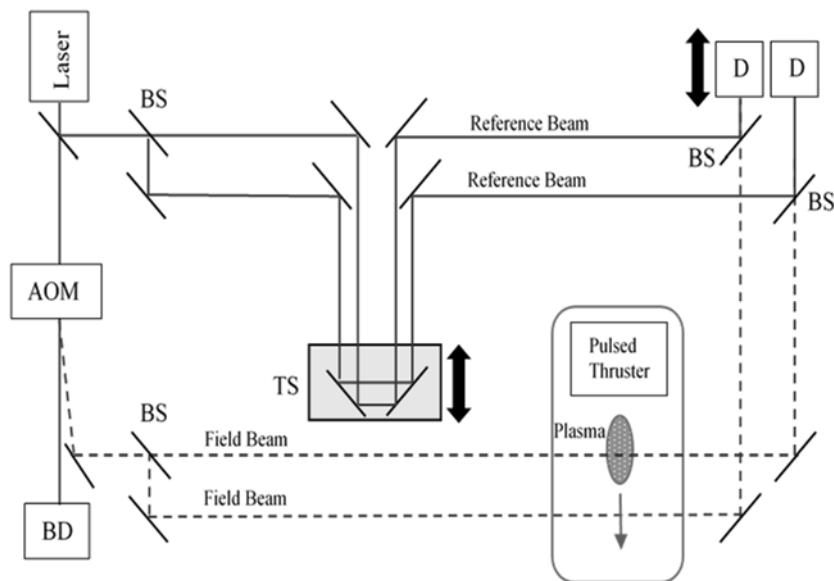
Figure 8. Schematic of heterodyne laser interferometer setup (double cord)

American Institute of Aeronautics and Astronautics
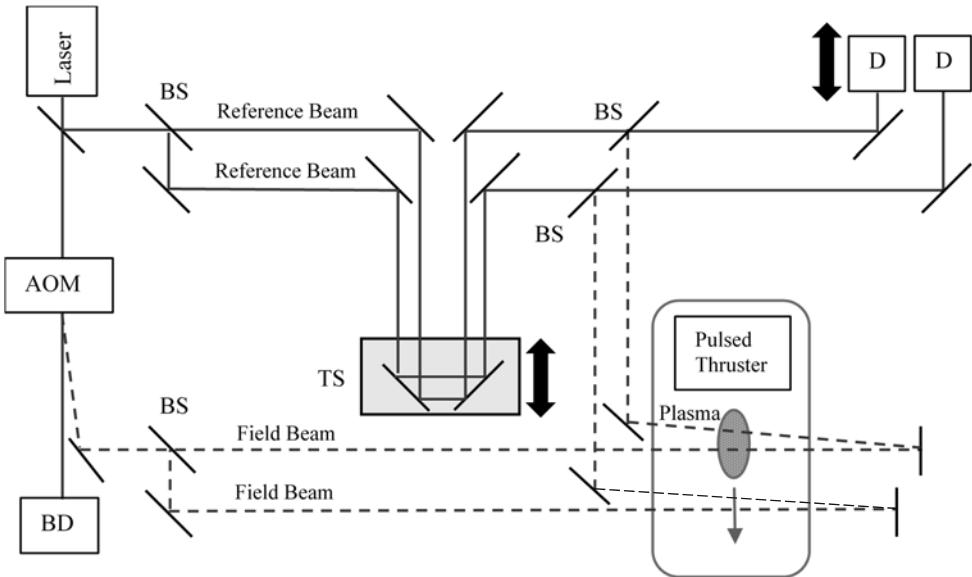
*Figure 9. Schematic of alternate heterodyne laser interferometer setup (double cord)*
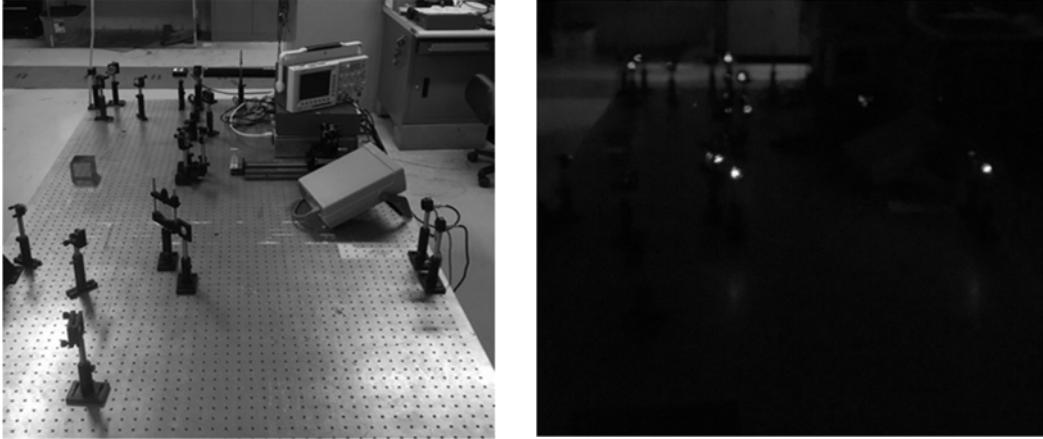
Figure 10. Photographs of heterodyne laser interferometer setup (double cord) in configuration shown in Figure 8

IV.   Summary

The purpose of this effort was to work towards the demonstration of an arcjet using green propellant. Tasks included development of two diagnostics tools to be used in performance evaluation—emission spectroscopy and heterodyne laser interfereometery. A two-cord heterodyne laser interferometer with electronic quadrature phase detection was demonstrated, and is ready for implementation. An emission spectroscopy setup is nearly completed and waiting for missing detector components. Imaging systems that will allow spatially resolved spectral images of thruster plumes were designed and components were ordered. Finally, an arcjet thruster was readied for testing with simulated ammonia and hydrazine propellants to establish baseline operation before moving on to a green propellant. The arcjet insulator was updated for swirling flow propellant injection. Improvements to ease assembly and increase insulator robustness were suggested.

References

1. *High Performance Green Propellant for Satellite.* Neff, K., King, P., Anflo, K., and Mollerberg, R. Denver : American Institute of Aeronautics and Astronautics, 2009. AIAA 2009-4878.

2. Jankovsky, Robert S. *HAN-Based Monopropellant Assessment for Spacecraft.* s.l. : NASA, 1996. NASA Technical Memorandum 107287.

3. Jahn, Robert G. *Physics of Electric Propulsion.* s.l. : Dover Publications, 2006.

4. Jahn, Robert G. and Choueiri, Edgar Y. Electric Propulsion. *Encyclopedia of Physical Science and Technology, Third Edition, Volume 5.* s.l. : Academic Press, 2002.

5. Lochte-Holtgreven, W. *Plasma Diagnostics.* New York, NY : Interscience (Wiley), 1968.

6. Griem, Hans R. *Principles of Plasma Spectroscopy (Cambridge Monographs on Plasma Physics).* Cambridge : Cambridge University Press, 2005.

7. Hecht, Eugene and Zajac, Alfred. *Optics.* Reading, Massachussetts : Addison-Wesley Publishing Co., 1974.

8. *Atomic Spectra Database, NIST Standard Reference Database 78.* s.l. : U.S. Department of Commerce , 2016.

9. Holt, E.H. and Haskel, R.E. *Foundations of Plasma Dynamics.* New York : MacMillan, 1965.

10. Smith, L.M., Keefer, D.R., and Wright, N.W. A fiber-optic interferometer for in-situ measurements of plasma number density in pulsed-power applications. *Review of Scientific Instruments.* July 2003, Vol. 74, 7.

11. Weber, B.V. and Hinshelwood, D.D. He–Ne interferometer for density measurements in plasma opening switch experiments. *Review of Scientific Instruments.* 1992, Vol. 63, 5199.

12. Weber, B.V, and Hinshelwood, D.D. Interferometry of flashboard and cable-gun plasma opening switches on Hawk. *IEEE Transactions on Plasma Science.* 1997, Vol. 25, 2.

13. Kumar, Deepak and Bellan, Paul M. Heterodyne interferometer with unequal path lengths. *Review of Scientific Instruments.* 2006, Vol. 77, 083503.

American Institute of Aeronautics and Astronautics